Am J Transl Res 2026;18(6):5165-5176
www.ajtr.org /ISSN:1943-8141/AJTR0171786

Original Article

Application value of CT-based extracellular volume fraction in assessing microsatellite status in colorectal cancer

Xiao-Ying Wang[1], Chang-Qing Pan[2], Shao-Ying Ling[2], Hong-Qiu Kuang[2], Sheng-Song Kuang[2], Li Peng[2], Wei Deng[1]

[1]Department of Radiology, Nanchang People's Hospital, Nanchang 330008, Jiangxi, China; [2]Department of Radiology, Xunwu People's Hospital, Xunwu 342200, Jiangxi, China

Received January 30, 2026; Accepted May 15, 2026; Epub June 15, 2026; Published June 30, 2026

Abstract: Objective: To investigate the application value of computed tomography (CT)-derived extracellular volume fraction (ECV) for predicting microsatellite instability (MSI) status in colorectal cancer (CRC). Methods: We enrolled a total of 121 consecutive patients with CRC who underwent curative resection. Prior to surgery, each patient underwent a contrast-enhanced CT scan for ECV quantification. MSI status was determined by immunohistochemistry or polymerase chain reaction. Univariate and multivariate techniques of logistic regression analysis were conducted to find the independent predictors. Three predictive models were developed and compared: ECV-only, clinical, and combined. Model performance was assessed using receiver operating characteristic curves, DeLong test, calibration curves, and decision curve analysis. Results: The mean ECV% of the MSI-high group (n = 28) was significantly higher than that of the MSS group (n = 84) (P<0.001). Significant difference was noted among MSI-H, MSI-L (n = 9), and MSS groups (F = 8.37; P<0.001). Based on multivariate analysis, tumor diameter ≥5 cm, N0 stage and higher ECV% were independent predictors. As per the results, the combination model had an AUC of 0.81 (95% CI: 0.72-0.90), which was higher than the other models but the differences were statistically not significant (P = 0.051 and P = 0.135). The model demonstrated solid calibration and positive net clinical benefit between 10% and 80% threshold probabilities. Conclusion: CT derived ECV is significantly associated with MSI status in CRC. A non-invasive preoperative model for predicting microsatellite instability that combines ECV, tumor diameter and N stage has a promising diagnostic accuracy.

Keywords: Colorectal cancer, extracellular volume fraction, microsatellite status, computed tomography

Introduction

The incidence and death rate of colorectal cancer (CRC) is high all over the world [1]. As the Global Burden of Disease report states, 1.9 million new cases of CRC were diagnosed in 2020 and this number will likely reach 3.2 million by 2024 [2]. In recent years, with the deepening of the concept of precision medicine, molecular subtyping of tumours has exerted a decisive influence on personalized treatment decision-making and prognostic prediction [3, 4]. Microsatellite instability (MSI) is an important molecular signature of CRC, which is a major biomarker for the screening of Lynch syndrome, and is strongly correlated with immunotherapy efficacy and prognosis [5, 6]. Studies show that patients with MSI-high (MSI-H) tumors have a significant increased rate of objective responses to PD-1/PD-L1 inhibitor therapy as compared to patients with MSI stable (MSS)/mismatch repair-proficient (pMMR) tumors [6, 7]. Thus, accurate preoperative evaluation of the MSI status has important clinical significance for personalized treatment strategies. Currently, the techniques for MSI detection especially gene sequencing or immunohistochemical detection have specifications. They are used in the advanced clinical detection. However, there are some limitations to the operation complexity, high cost and sample collection dependence.

The Extracellular Volume Fraction (ECV), as an imaging parameter for quantitatively evaluating the interstitial components of tissues, has dem-

https://doi.org/10.62347/GFEQ3487

onstrated unique value in the study of the tumor microenvironment [8]. ECV, when combined with CT contrast enhancement and corrected for serum iodine concentration, can reflect pathophysiological alterations such as tumor stromal fibrosis, oedema, and angiogenesis [9]. Studies have shown that MSI is closely related to the immune microenvironment of CRC, which may lead to characteristic changes in ECV values [10, 11]. Previous studies have confirmed that ECV has significant value in the pathological classification and prognosis assessment of malignant tumors such as liver cancer and lung cancer [12, 13]. However, there are limited reports on the role of ECV in the determination of MSI status in CRC, and the potential association mechanism between it and the tumor immune microenvironment and genetic instability still needs to be explored.

Based on the above background, this study aims to deeply explore the application value of ECV based on CT in predicting the microsatellite state of CRC. We hypothesize that due to its lymphocyte-rich microenvironment characteristics, the ECV value of MSI-H type CRC will be significantly different from that of MSS type tumors. The results of this study are expected to provide a non-invasive and convenient MSI status screening tool based on conventional CT examination for clinical practice, thereby offering important imaging evidence for the molecular typing of colorectal cancer patients and the early formulation of individualized treatment strategies without the need for additional invasive operations.

Materials and methods

Research subjects

This retrospective study consecutively enrolled patients with colorectal cancer who were diagnosed at Nanchang People's Hospital and Xunwu People's Hospital, and underwent curative resection between January 2018 and March 2025. After rigorous screening, 121 patients were included in the final analysis. The study protocol complied with the principles of the Declaration of Helsinki and was approved by the Medical Ethics Committee of Nanchang People's Hospital.

Inclusion and exclusion criteria

All patients met the following inclusion criteria: (1) postoperative pathology confirmed primary CRC; (2) patients who completed an enhanced abdominal CT scan within one month before the operation; (3) postoperative tissue specimens were detected by immunohistochemistry (IHC) or polymerase chain reaction (PCR) to determine the MSI status; (4) patients with complete clinical and postoperative care data. The exclusion criteria for patients are as follows: (1) patients who received radiotherapy, chemotherapy, targeted therapy or immunotherapy before the operation; (2) patients with poor CT image quality; (3) patients with other malignant tumors or systemic diseases.

CT examination and ECV measurement

All patients underwent abdominal enhanced CT scans using a GE Revolution 256-slice spiral CT. Scan parameters: Tube voltage of 120 kV, tube current using automatic tube current modulation (Care Dose 4D), slice thickness of 0.625 mm, slice interval of 0.625 mm, matrix of 512×512, and field of view (FOV) of 350-400 mm. Enhanced scan protocol: Non-ionic contrast agent (iohexol, 350 mgI/mL) was injected via the antecubital vein at a rate of 3.0-3.5 mL/s with a dose of 1.5 mL/kg. Three-phase scans were performed at 30-35 s (arterial phase), 60-70 s (portal venous phase), and 120-150 s (delayed phase) after injection, respectively. The original image data were transmitted to the AW 4.7 post-processing workstation for multiplanar reconstruction (MPR) to clearly display the tumor lesions.

ECV measurement was independently completed by two radiologists with more than 5 years of experience in abdominal imaging diagnosis using the double-blind method. Disagreements were resolved through departmental consultation. Specific steps: (1) On the portal venous phase images, three regions of interests (ROIs) (area of 20-30 mm^2) were selected in the tumor parenchyma, avoiding necrotic areas, calcifications, blood vessels, and intestinal contents; (2) One ROI was selected in the abdominal aorta at the same level as a reference for arterial blood pool, and one ROI was selected in the erector spinae muscle as a reference for normal soft tissue; (3) The pre-contrast CT value (HUpre) and post-contrast CT value (HUenh) of each ROI were extracted using the quantitative analysis software built into the workstation; (4) ECV was calculated according to the formula: ECV = (1 - Hct) × (HUenh - HUpre)tumor/(HUenh - HUpre) arterial blood pool, where Hct was the hematocrit value detected by routine blood test

on the day of the patient's examination. Finally, the average ECV value of the three tumor ROIs was taken as the final ECV value of the patient. Inter- and intra-observer agreement were assessed using the intraclass correlation coefficient (ICC), with ICC>0.75 indicating good consistency.

MSI status detection and grouping

The postoperative tumor tissues were used to determine the MSI status following standard clinical protocols [14]. An initial screening was performed using immunohistochemistry (IHC) for four mismatch repair [15, 16]. Any loss of protein expression will be classified as MMR deficient (dMMR) and has been considered equivalent to MSI-high (MSI-H). To confirm the MSI status of cases with intact protein expression, analysis by polymerase chain reaction (PCR) of standard microsatellite loci was conducted [17]. Patients were classified as MSI-H if they exhibit high instability and identified as microsatellite stable (MSS) if they exhibit low instability or stability. For the statistical analyses, the MSI cohort only included the MSI-H cases (n = 28), while the MSS cohort consisted of both MSS and MSI-L cases (n = 93).

Data collection

The following data were extracted from the electronic medical record system: (1) Demographic characteristics: age, gender, BMI; (2) Tumor characteristics: location (right colon/left colon/rectum), size (maximum diameter), TNM staging (per the 8th edition of the American Joint Committee on Cancer (AJCC) Cancer Staging Manual) [18], differentiation grade (moderately/highly differentiated vs. poorly differentiated), lesion type (ulcerative vs. non-ulcerative), and vascular invasion (present vs. absent); (3) Laboratory indicators: preoperative haematocrit, carcinoembryonic antigen (CEA), and carbohydrate antigen 19-9 (CA19-9) levels.

Statistical analysis

Statistical analyses were performed using SPSS 26.0 (IBM Corp., Armonk, NY, USA) and R 4.2.1 (R Foundation for Statistical Computing, Vienna, Austria), with a two-tailed P<0.05 considered statistically significant. Continuous variables were tested for normality via Shapiro-Wilk test; normally distributed data were expressed as mean ± standard deviation ($\bar{x} \pm s$) and compared using independent samples t-test, while non-normally distributed data were presented as median (interquartile range) [M (Q1, Q3)] and analyzed with Mann-Whitney U test. Categorical variables were described as n (%) and compared using x^2 test or Fisher's exact test as appropriate. Intraclass correlation coefficient (ICC) >0.75 indicated good intra- and inter-observer consistency for ECV measurements. For subgroup analyses comparing ECV% among MSI-H, MSI-L, and MSS groups, one-way ANOVA was used to assess overall differences, followed by LSD-t test for post-hoc pairwise comparisons when the ANOVA result was statistically significant. Univariate Logistic regression screened variables for three prediction models: Model A (ECV alone), Model B (clinical indicators, backward stepwise multivariate Logistic regression), and Model C (ECV + Model B independent factors). Receiver operating characteristic (ROC) curves, Delong test, calibration curves (Hosmer-Lemeshow test), and bootstrap validation (1,000 repetitions) evaluated model performance. Restricted cubic splines (RCS) were used to analyze the nonlinear association between ECV and MSI risk (adjusted for age and gender), and decision curve analysis (DCA) was used to analyze clinical net benefit.

Results

Patient demographics and baseline characteristics

A total of 121 CRC patients were included in this study. The cohort comprised 68 (56.20%) males and 53 (43.80%) females, with a mean age of 65.07 ± 13.21 years. According to the postoperative MSI status, patients were categorized into an MSS group (n = 93) and an MSI group (n = 28). The comparison of baseline clinical-pathological features between the two groups is summarized in **Table 1**. Patients in the MSI group had a higher proportion of tumors with a diameter ≥5 cm (71.43% vs. 37.63%, P = 0.002), were more likely to have right-sided colon cancers (71.43% vs. 49.46%, P = 0.041), and had a lower proportion of lymph node metastases (N1-2 stage: 28.57% vs. 60.22%, P = 0.003).

Comparison of ECV% between MSS and MSI groups

CT-derived ECV% was successfully measured in all patients with excellent inter- and intra-observer agreement (ICC>0.85). Representative

Table 1. Baseline characteristics of colorectal cancer patients stratified by microsatellite instability status

Variables	Total (n = 121)	MSS group (n = 93)	MSI group (n = 28)	Statistic	*P*
Age, Mean ± SD	65.07 ± 13.21	64.34 ± 13.69	67.50 ± 11.37	t = -1.11	0.270
Gender, n (%)				χ^2 = 0.30	0.583
Female	53 (43.80)	42 (45.16)	11 (39.29)		
Male	68 (56.20)	51 (54.84)	17 (60.71)		
Tumor diameter, n (%)				χ^2 = 9.91	0.002
<5 cm	66 (54.55)	58 (62.37)	8 (28.57)		
≥5 cm	55 (45.45)	35 (37.63)	20 (71.43)		
Tumor location, n (%)				χ^2 = 4.19	0.041
Left	55 (45.45)	47 (50.54)	8 (28.57)		
Right	66 (54.55)	46 (49.46)	20 (71.43)		
Lesion type, n (%)				χ^2 = 0.34	0.561
Non-ulcerative	62 (51.24)	49 (52.69)	13 (46.43)		
Ulcerative	59 (48.76)	44 (47.31)	15 (53.57)		
Differentiated degree, n (%)				χ^2 = 2.45	0.117
Moderately/highly	95 (78.51)	76 (81.72)	19 (67.86)		
Low	26 (21.49)	17 (18.28)	9 (32.14)		
Vascular invasion, n (%)				χ^2 = 0.11	0.745
No	79 (65.29)	60 (64.52)	19 (67.86)		
Yes	42 (34.71)	33 (35.48)	9 (32.14)		
T stage, n (%)				χ^2 = 0.00	1.000
T_{1-2}	18 (14.88)	14 (15.05)	4 (14.29)		
T_{3-4}	103 (85.12)	79 (84.95)	24 (85.71)		
N stage, n (%)				χ^2 = 8.65	0.003
N_0	57 (47.11)	37 (39.78)	20 (71.43)		
N_{1-2}	64 (52.89)	56 (60.22)	8 (28.57)		
CEA, n(%)				χ^2 = 1.73	0.189
<5 ng/mL	65 (53.72)	53 (56.99)	12 (42.86)		
≥5 ng/mL	56 (46.28)	40 (43.01)	16 (57.14)		
CA199, n(%)				χ^2 = 1.37	0.243
<28 U/mL	72 (59.50)	58 (62.37)	14 (50.00)		
≥28 U/mL	49 (40.50)	35 (37.63)	14 (50.00)		

Abbreviations: MSI, microsatellite instability; MSS, microsatellite stable; SD, standard deviation; CEA, carcinoembryonic antigen; CA19-9, carbohydrate antigen 19-9.

CT images demonstrating ECV% measurement in MSI and MSS tumors are shown in **Figure 1**. The mean ECV% was significantly higher in the MSI group compared to the MSS group (36.15% ± 6.42% vs. 30.82% ± 5.91%, *P*<0.001) (**Figure 2**).

Subgroup analysis of ECV% across MSI-H, MSI-L, and MSS groups

To further explore the biological gradient of ECV, a subgroup analysis was carried out to compare the ECV values of the MSI-H (n = 28), MSI-L (n = 9), and MSS (n = 84) groups. The mean ECV% was found to be 36.15% ± 6.42% in the MSI-H group, 31.29% ± 3.28% in the MSI-L group and 30.76% ± 6.14% in the MSS group. The study found that the means of the three groups were significantly different (F = 8.37, P<0.001). Results of post-hoc pairwise comparisons with LSD-t test reveal that ECV% of MSI-H tumors was significantly higher than that of MSI-L tumors (P = 0.039) and MSS tumors (P<0.001). No statistically significant difference was observed between MSI-L and MSS groups (P = 0.804) (**Figure 3**). These

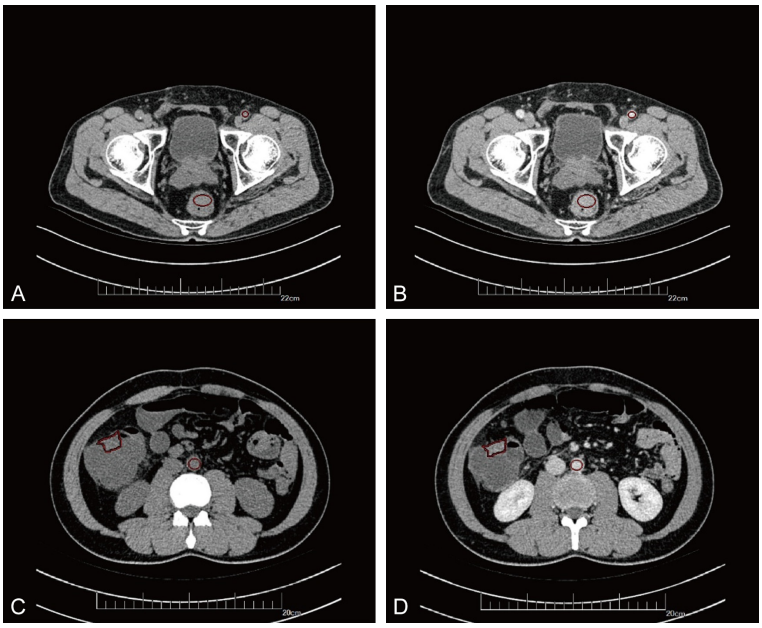

Figure 1. Representative CT images of ECV measurement in MSS and MSI colorectal cancer. A, B. Pre-contrast and portal venous phase CT images of an MSS tumor (rectal anterior wall) with an ECV of 28.8%; C, D. Pre-contrast and portal venous phase CT images of an MSI tumor (ascending colon anterior wall) with an ECV of 42.9%. Abbreviations: ECV, extracellular volume fraction; MSS, microsatellite stable; MSI, microsatellite instability; CT, computed tomography.

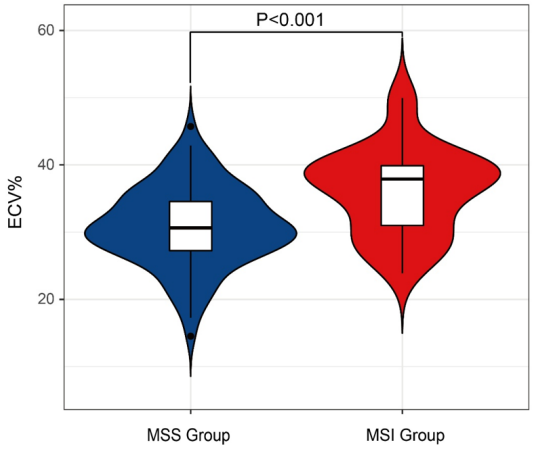

Figure 2. Comparison of CT-derived ECV between MSS and MSI groups. Abbreviations: ECV, extracellular volume fraction; MSS, microsatellite stable; MSI, microsatellite instability; CT, computed tomography.

results indicate that a biological gradient for extracellular volume fraction exists across the MSI spectrum; specifically, interstitial changes were most pronounced in MSI-H tumors and less heightened in MSI-L tumors that did not differ significantly from MSS tumors.

Association between ECV% and MSI risk

A dose-response relationship between ECV% and the risk of MSI was evaluated using restricted cubic spline analysis, with adjustment for age and gender (**Figure 4**). The overall association was statistically significant (P for overall = 0.005), indicating that the probability of MSI increased with rising ECV%. No evidence of a non-linear relationship was detected (P for non-linearity = 0.764).

Identification of independent clinical predictors for MSI status

Univariate and multivariate Logistic regression analyses were conducted to screen clinical factors associated with MSI status (**Table 2**). In the univariate Logistic regression analysis, tumor diameter (≥5 cm vs. <5 cm: OR = 4.14, 95% CI: 1.65-10.41, P = 0.002), tumor location (right vs. left: OR = 2.55, 95% CI: 1.02-6.38, P = 0.045), and N stage (N1-2 vs. N0: OR = 0.26, 95% CI: 0.11-0.66, P = 0.005) were significantly associated with MSI status (P<0.05). These variables were further included in the multivariate Logistic regression analysis using the backward stepwise method. Finally, tumor diameter (≥5 cm vs. <5 cm: OR = 4.19, 95% CI: 1.61-10.87, P = 0.003) and N stage (N1-2 vs. N0: OR = 0.26, 95% CI: 0.10-0.68, P = 0.006) were identified as independent predictive factors for MSI status, forming the clinical prediction model.

Development and presentation of a combined prediction model incorporating ECV%

A multivariate logistic regression analysis of ECV% value with the two independents clinical predictors mentioned above (tumor diameter, N stage) was conducted to derive a combined predictive model (**Table 3**). According to this combined model, independent predictors of active contralateral disease include higher

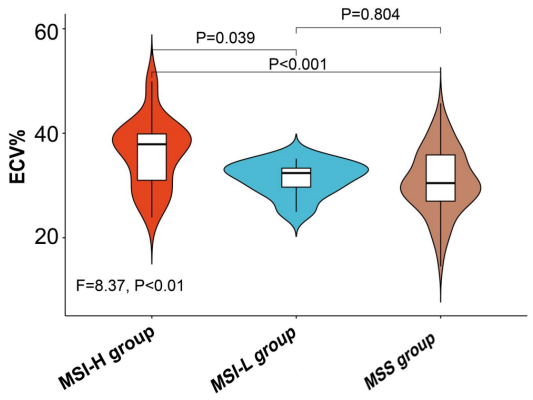

Figure 3. Comparison of CT-derived ECV% among MSI-H, MSI-L, and MSS subgroups. *P* values for pairwise comparisons were derived from LSD-t test. Abbreviations: ECV, extracellular volume fraction; MSI-H, microsatellite instability-high; MSI-L, microsatellite instability-low; MSS, microsatellite stable.

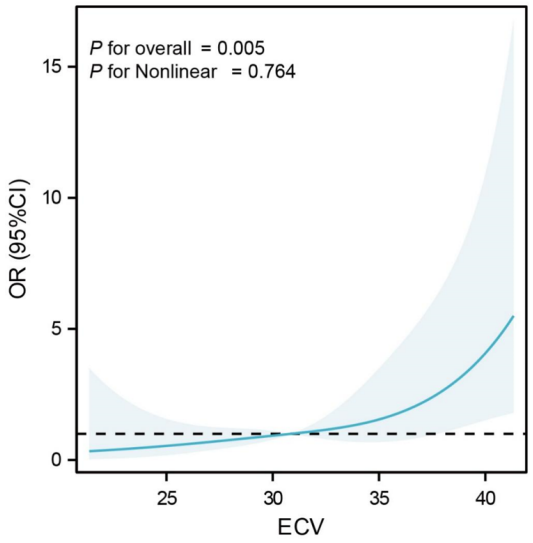

Figure 4. Restricted cubic spline analysis of the dose-response relationship between ECV and MSI risk. Abbreviations: ECV, extracellular volume fraction; MSI, microsatellite instability; OR, odds ratio; CI, confidence interval.

ECV% (OR = 1.15, 95% CI: 1.05-1.26, P = 0.002), tumor diameter ≥5 cm (OR = 3.59, 95% CI: 1.30-9.87, P = 0.013), and N1-2 stage (OR = 0.24, 95% CI: 0.08-0.67, P = 0.006). In order to facilitate its use in clinical practice, we created a nomogram that uses these three variables to estimate the individual probability of MSI visually (**Figure 5**).

Diagnostic performance and comparison of the three prediction models

The diagnostic performance of the three models was evaluated using ROC analysis (**Figure 6A**). The combined model demonstrated the highest predictive efficacy with an AUC of 0.81 (95% CI: 0.72-0.90). The clinical model (AUC = 0.74, 95% CI: 0.62-0.85) and the ECV-only model (AUC = 0.73, 95% CI: 0.61-0.84) exhibited comparable performance. Pairwise comparison of the AUCs using DeLong's test (**Table 4**) revealed that the AUC of the combined model was numerically higher than that of the clinical model (difference = 0.076, *P* = 0.051) and the ECV-only model (difference = 0.084, *P* = 0.135), though these differences did not achieve statistical significance and should be interpreted with caution. No significant difference was found between the clinical model and the ECV-only model (AUC difference = 0.008, *P* = 0.930).

Calibration and internal validation of the combined prediction model

The calibration curve of the combined model showed good agreement between the predicted probability and the actual observed frequency of MSI status, which was confirmed by a non-significant Hosmer-Lemeshow test (*P* = 0.511) (**Figure 6B**). Internal validation using the bootstrap resampling method (1,000 repetitions) further confirmed the robustness of the model, yielding an optimism-corrected AUC of 0.86 (95% CI: 0.82-0.90) (**Figure 7A**). The calibration curve after internal validation also indicated excellent fit (Hosmer-Lemeshow *P* = 0.807) (**Figure 7B**).

Clinical utility of the combined prediction model

Decision curve analysis was performed to assess the clinical net benefit of the combined prediction model across a range of threshold probabilities (**Figure 8**). The analysis demonstrated that using the combined model to guide clinical decisions would provide a net benefit over the strategies of "treating all" or "treating none" when the risk threshold for considering a patient as high-risk for MSI is between 10% and 80%. This indicates the potential clinical utility of the model for non-invasive MSI screening in a substantial portion of the patient population.

Discussion

CRC is a malignant tumor with a persistently high incidence and mortality rate worldwide

Table 2. Univariate and multivariate logistic regression analysis of clinical factors associated with microsatellite instability in colorectal cancer

Variables	Univariate					Multivariate				
	β	S.E.	Z	*P*	OR (95% CI)	β	S.E.	Z	*P*	OR (95% CI)
Age	0.02	0.02	1.11	0.268	1.02 (0.99-1.05)					
Gender										
Female					1.00 (Reference)					
Male	0.24	0.44	0.55	0.583	1.27 (0.54-3.01)					
Tumor diameter										
<5 cm					1.00 (Reference)					1.00 (Reference)
≥5 cm	1.42	0.47	3.02	0.002	4.14 (1.65-10.41)	1.43	0.49	2.94	0.003	4.19 (1.61-10.87)
Tumor location										
Left					1.00 (Reference)					
Right	0.94	0.47	2.01	0.045	2.55 (1.02-6.38)					
Lesion type										
Non-ulcerative					1.00 (Reference)					
Ulcerative	0.25	0.43	0.58	0.562	1.28 (0.55-3.00)					
Differentiated degree										
Moderately/highly					1.00 (Reference)					
Low	0.75	0.49	1.55	0.122	2.12 (0.82-5.48)					
Vascular invasion										
No					1.00 (Reference)					
Yes	-0.15	0.46	-0.33	0.745	0.86 (0.35-2.12)					
T stage										
T_{1-2}					1.00 (Reference)					
T_{3-4}	0.06	0.61	0.10	0.920	1.06 (0.32-3.54)					
N stage										
N_0					1.00 (Reference)					1.00 (Reference)
N_{1-2}	-1.33	0.47	-2.84	0.005	0.26 (0.11-0.66)	-1.34	0.49	-2.75	0.006	0.26 (0.10-0.68)
CEA										
<5 ng/mL					1.00 (Reference)					
≥5 ng/mL	0.57	0.44	1.31	0.191	1.77 (0.75-4.15)					
CA199										
<28 U/mL					1.00 (Reference)					
≥28 U/mL	0.51	0.43	1.16	0.245	1.66 (0.71-3.88)					

Abbreviations: β, regression coefficient; S.E., standard error; OR, odds ratio; CI, confidence interval; CEA, carcinoembryonic antigen; CA19-9, carbohydrate antigen 19-9.

[19]. Precise molecular typing is of decisive significance for the formulation of individualized treatment plans and prognosis assessment [20]. Among them, MSI, as a key molecular marker of CRC, is closely related to the therapeutic efficacy and prognosis [21]. The ECV, as an imaging parameter quantifying the composition of the tissue interstitium, has demonstrated value in the pathological classification and prognostic assessment of malignant tumors such as hepatocellular carcinoma and lung cancer [22, 23]. However, its application in determining MSI status in CRC remains to be clarified. This retrospective analysis of clinical and imaging data from 121 colorectal cancer patients revealed significantly higher ECV values in the MSI group compared to the MSS group. Furthermore, ECV demonstrated a linear correlation with MSI risk. A further constructed combined predictive model incorporating 'ECV + tumor diameter + N staging' achieved an AUC of 0.81 which increased to 0.86 (95% CI: 0.82-0.90) after internal validation via Bootstrap sampling. This model demonstrated significant clinical net benefit within the 0.1-0.8 high-risk threshold range, offering a novel non-invasive approach for assessing MSI status in CRC.

The result of a significant increase in ECV values in the MSI group in this study can be ex-

Table 3. Multivariate Logistic regression analysis of the combined prediction model for MSI status

Variables	β	S.E.	Z	*P*	OR (95% CI)
Intercept	-5.97	1.58	-3.77	<0.001	0.00 (0.00-0.06)
Tumor diameter					
<5 cm					1.00 (Reference)
≥5 cm	1.28	0.52	2.47	0.013	3.59 (1.30-9.87)
N stage					
N_0					1.00 (Reference)
N_{1-2}	-1.44	0.53	-2.72	0.006	0.24 (0.08-0.67)
ECV	0.14	0.05	3.07	0.002	1.15 (1.05-1.26)

Abbreviations: β, regression coefficient; S.E., standard error; OR, odds ratio; CI, confidence interval; ECV, extracellular volume fraction.

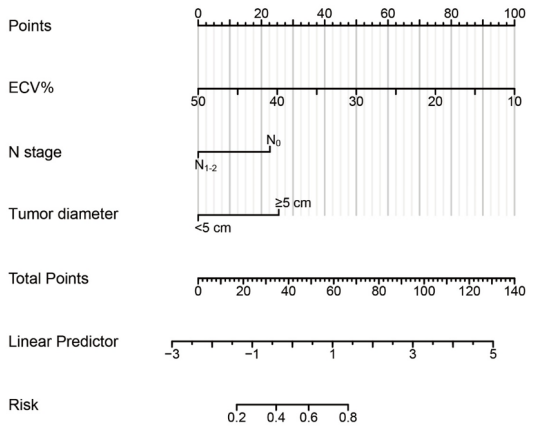

Figure 5. Nomogram of the combined prediction model for predicting MSI status in colorectal cancer. Abbreviations: ECV, extracellular volume fraction; MSI, microsatellite instability.

plained by the pathophysiological mechanism of the tumor microenvironment. Previous studies have demonstrated that MSI-H colorectal cancer exhibits an immune microenvironment characterized by 'abundant lymphocytic infiltration' [24, 25]. Tumor cells accumulate numerous mutations due to mismatch repair defects, generating tumor-associated antigens that activate the body's anti-tumor immune response [26]. This leads to the recruitment of substantial numbers of immune cells (such as CD8+ T cells and macrophages) to the tumor stroma, accompanied by increased stromal fibrosis and abnormal angiogenesis [27]. Through enhanced CT scanning in conjunction with serum iodine concentration correction, ECV can quantitatively reflect the proportion of interstitial tissue components [28]. Greater infiltration of immune cells and stromal fibrosis directly leads to expanded extracellular space in the tissues which is reflected as greater ECV values. The findings by Zhang et al. [9] predict the tumor-to-stroma ratios in CRC. They show that the ECV value indirectly correlates with the biological behavior of the tumor. This is by reflecting the extent of stromal fibrosis. Moreover, RCS analysis of ECV showed a linear association with MSI risk, pointing towards elevated ECV values being a dose-dependent feature of MSI status. The study findings provide further justification for the use of ECV as a MSI assessment measure. Earlier studies were only concerned with whether differences exist or not, failing to consider the underlying pattern responsible.

In terms of model construction and comparison, this study combines ECV with clinicopathological features for a comprehensive analysis. From a clinical perspective, this study found that the MSI group exhibited a higher proportion of tumors with a diameter ≥5 cm, a greater incidence in the right-sided colon, and a higher prevalence of N0 staging. These results are consistent with previous research findings. Fujiyoshi et al. [29] reported an independent predictor of MSI-H status in CRC patients with a tumor diameter of ≥6 cm. Karavin et al. [30] found through a study of 101 CRC patients that tumors in MSI-H type patients were more likely to occur in the right colon, and there was statistical significance. In addition, Lu et al. [31] also found a significant association between MSI and tumor location, tumor diameter, and lymphatic metastasis, which is similar to the results of this study. It is worth noting that the N_{1-2} stage is negatively correlated with the MSI status, meaning that lymph node metastasis is less common in MSI-type CRC. This result supports the clinical observation that MSI-H-type CRC may have relatively inert biological behavior [32]. In addition, Wang et al. [33] found that the MSI group had more tertiary lymphocyte structures and higher maturity, as well as a higher proportion of CD8+ T cells, which they speculated might be related to the activation of the local anti-tumor immune response promoted by MSI. When ECV is combined with these

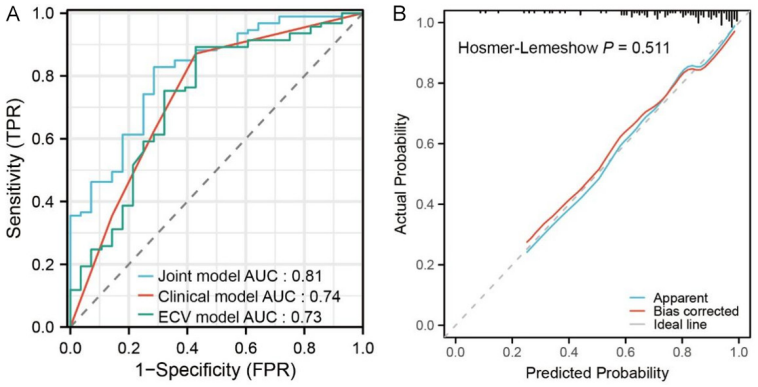

Figure 6. Performance evaluation of the prediction models. A. ROC curves of the ECV-only model (AUC = 0.73), clinical model (AUC = 0.74), and combined model (AUC = 0.81); B. Calibration curve of the combined model. Abbreviations: ECV, extracellular volume fraction; MSI, microsatellite instability; ROC, receiver operating characteristic; AUC, area under the curve; TPR, true positive rate; FPR, false positive rate.

Table 4. Comparison of diagnostic efficacy among the three prediction models using DeLong test

Model 1	Model 2	AUC difference	Statistics	*P* value
Joint model	Clinical model	0.076	1.95	0.051
Joint model	ECV model	0.084	1.50	0.135
Clinical model	ECV model	0.008	0.09	0.930

Abbreviations: AUC, area under the curve; ECV, extracellular volume fraction.

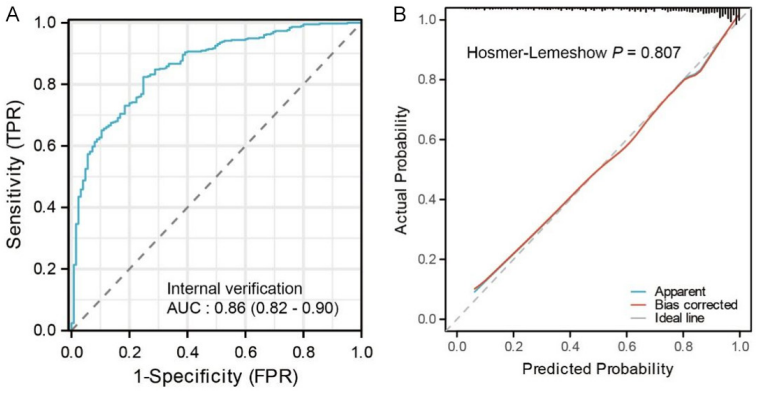

Figure 7. Internal validation of the combined prediction model. A. ROC curve after bootstrap resampling (1,000 repetitions); B. Calibration curve after internal validation. Abbreviations: ECV, extracellular volume fraction; MSI, microsatellite instability; ROC, receiver operating characteristic; AUC, area under the curve; TPR, true positive rate; FPR, false positive rate.

two powerful clinical predictors, the diagnostic efficacy of the combined model shows a numerical improving trend compared with the individual clinical models or ECV models. Although the DeLong test indicated that the AUC differences did not reach statistical significance (likely due to limited sample size), the calibration curve demonstrated good fitting and the decision curve analysis showed positive net clinical benefit, suggesting that the addition of ECV may provide valuable supplementary information for prediction. However, we acknowledge that the absence of statistical significance requires cautious interpretation of these findings.

Naturally, this study also presents several limitations. Firstly, as a single-center retrospective investigation, selection bias may be present. The sample size, although selected based on strict inclusion and exclusion criteria, remains small (particularly MSI group n = 28), potentially limiting statistical power and model generalizability. There is a need for multicenter, prospective studies with larger cohorts for external validation. Furthermore, CT values that are used for calculating for ECV will are those obtained at equilibrium. Above and beyond this technical note, other factors can contribute to the accuracy of these CT values. These include scanning protocols (like contrast agent dosage or injection rate and scanning timing), the patient's cardiac output, and the patient's hemostatic status. Notwithstanding the fact that we use a standardized scanning protocol and calibrate with the abdominal aorta as a blood pool reference, we must still be aware of the differences due to the CT scanner model and reconstruction algorithm. Third, MSI-L with MSS was combined while this study denoted MSI-H as the MSI type. The MSI-H category is likely the main immunotherapy beneficiary, but the classification may underestimate the biological properties of the MSI-L. Future studies might analyze the variations and differences of ECV between different microsatellite status. Fourth,

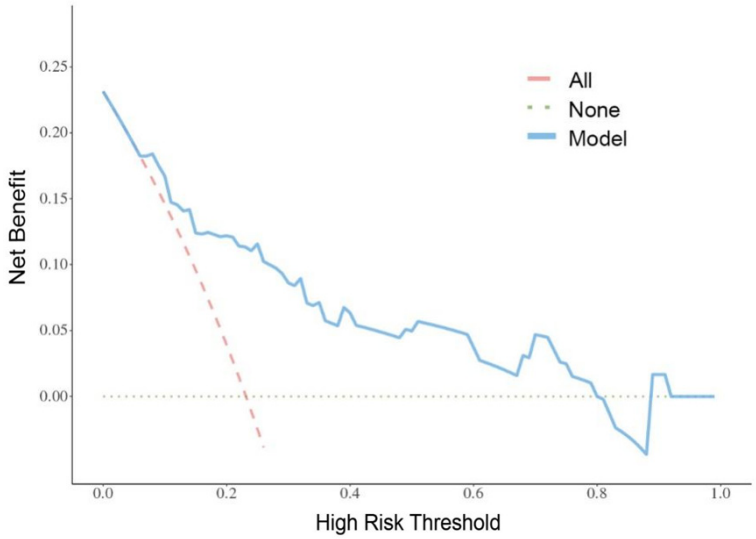

Figure 8. Decision curve analysis of the combined prediction model.

this study used ECV as the only quantitative imaging index without using any CT morphological features (such as tumor morphology, margin characteristics, enhancement patterns), texture features, or radiomics features. It is possible that the non-inclusion of information from extra imaging associated with microsatellite instability status restricted the model, further improving diagnostic performance. Future research should combine multi-dimensional imaging features and ECV to create radiomics models that incorporate clinical indicators. Fifth, although the combined model demonstrated the highest AUC (0.81) compared to the clinical model (0.74) and ECV-only model (0.73), the DeLong test did not reach statistical significance (P = 0.051 and P = 0.135, respectively). Therefore, we acknowledge that the observed numerical improvement in diagnostic efficacy should be interpreted with caution, and this lack of statistical significance may be attributed to the relatively small sample size. Sixth, the limited number of early-stage CRC cases (T1-T2 stage, n = 18, 14.88%) in this cohort precluded a reliable evaluation of ECV's predictive value for MSI status in early-stage tumors. Given that non-invasive molecular subtyping is equally critical for treatment decision-making in early-stage CRC, future research should expand the sample size of early-stage cases to specifically explore the application value of ECV in this population.

Conclusion

To summarize, the aforementioned study verifies that the ECV obtained from CT is positively and significantly correlated to MSI status in CRC and it was also an independent radiological marker to predict MSI. The integrated predictive model of tumor diameter and N staging presents with favorable diagnostic performance and clinical value, representing a novel feasible innovative tool for preoperative non-invasive assessment of CRC molecular subtyping. Further validation in large prospective studies is still warranted. Nonetheless, results of the analysis can help guide the image-based quantitative analyses of the tumor microenvironment and the early development of personalized treatment strategies.

Disclosure of conflict of interest

None.

Address correspondence to: Wei Deng, Department of Radiology, Nanchang People's Hospital, No. 2 Xiangshan South Road, Xihu District, Nanchang 330008, Jiangxi, China. Tel: +86-0791-86623952; E-mail: dengwei3366yxk@163.com

References

[1] Klimeck L, Heisser T, Hoffmeister M and Brenner H. Colorectal cancer: a health and economic problem. Best Pract Res Clin Gastroenterol 2023; 66: 101839.

[2] Morgan E, Arnold M, Gini A, Lorenzoni V, Cabasag CJ, Laversanne M, Vignat J, Ferlay J, Murphy N and Bray F. Global burden of colorectal cancer in 2020 and 2040: incidence and mortality estimates from GLOBOCAN. Gut 2023; 72: 338-344.

[3] Kiran NS, Yashaswini C, Maheshwari R, Bhattacharya S and Prajapati BG. Advances in precision medicine approaches for colorectal cancer: from molecular profiling to targeted therapies. ACS Pharmacol Transl Sci 2024; 7: 967-990.

[4] Muradi Muhar A, Velaro AJ, Prananda AT, Nugraha SE, Halim P and Syahputra RA. Precision

medicine in colorectal cancer: genomics profiling and targeted treatment. Front Pharmacol 2025; 16: 1532971.
[5] Staninova-Stojovska M, Matevska-Geshkovska N, Krstevska-Bozhinovikj E, Jovanovic R, Kubelka Sabit K, Angelovska B, Mitreski N and Dimovski A. Quantification of microsatellite instability testing and detection of lynch syndrome: step forward in improving mismatch repair testing in clinical practice. JCO Precis Oncol 2025; 9: e2400901.
[6] Xu Y, Liu K, Li C, Li M, Zhou X, Sun M, Zhang L, Wang S, Liu F and Xu Y. Microsatellite instability in mismatch repair proficient colorectal cancer: clinical features and underlying molecular mechanisms. EBioMedicine 2024; 103: 105142.
[7] Wu H, Deng M, Xue D, Guo R, Zhang C, Gao J and Li H. PD-1/PD-L1 inhibitors for early and middle stage microsatellite high-instability and stable colorectal cancer: a review. Int J Colorectal Dis 2024; 39: 83.
[8] Muthalaly RG, Tan S, Nelson AJ, Abrahams T, Han D, Tamarappoo BK, Dey D, Nicholls SJ, Lin A and Nerlekar N. Variation of computed tomography-derived extracellular volume fraction and the impact of protocol parameters: a systematic review and meta-analysis. J Cardiovasc Comput Tomogr 2024; 18: 457-464.
[9] Zhang Y, Zhang H, Li D, Yuan L, Deng L, Han T, Jing M, Zhang C, Zhang B and Zhou J. Contrast-enhanced CT-derived extracellular volume fraction in preoperative prediction of tumor-stroma ratio in colorectal cancer. Abdom Radiol (NY) 2026; 51: 639-649.
[10] Greco L, Rubbino F, Dal Buono A and Laghi L. Microsatellite instability and immune response: from microenvironment features to therapeutic actionability-lessons from colorectal cancer. Genes (Basel) 2023; 14: 1169.
[11] Bai J, Chen H and Bai X. Relationship between microsatellite status and immune microenvironment of colorectal cancer and its application to diagnosis and treatment. J Clin Lab Anal 2021; 35: e23810.
[12] Fu X, Guo Y, Zhang K, Cheng Z, Liu C, Ren Y, Miao L, Liu W, Jiang S, Zhou C, Su Y and Yang L. Prognostic impact of extracellular volume fraction derived from equilibrium contrast-enhanced CT in HCC patients receiving immune checkpoint inhibitors. Sci Rep 2025; 15: 13643.
[13] Jiang X, Ma Q, Zhou T, Feng Q, Yang W, Zhou X, Huang W, Lin X, Li J, Zhang X, Liu S, Xin X and Fan L. Extracellular volume fraction as a potential predictor to differentiate lung cancer from benign lung lesions with dual-layer detector spectral CT. Quant Imaging Med Surg 2023; 13: 8121-8131.
[14] Yuan Ying. Chinese expert consensus on microsatellite instability detection of colorectal cancer and other related solid tumors. Journal of Practical Oncology 2019; 34: 381-389.
[15] Umar A, Boland CR, Terdiman JP, Syngal S, de la Chapelle A, Rüschoff J, Fishel R, Lindor NM, Burgart LJ, Hamelin R, Hamilton SR, Hiatt RA, Jass J, Lindblom A, Lynch HT, Peltomaki P, Ramsey SD, Rodriguez-Bigas MA, Vasen HF, Hawk ET, Barrett JC, Freedman AN and Srivastava S. Revised Bethesda Guidelines for hereditary nonpolyposis colorectal cancer (Lynch syndrome) and microsatellite instability. J Natl Cancer Inst 2004; 96: 261-268.
[16] Sargent DJ, Marsoni S, Monges G, Thibodeau SN, Labianca R, Hamilton SR, French AJ, Kabat B, Foster NR, Torri V, Ribic C, Grothey A, Moore M, Zaniboni A, Seitz JF, Sinicrope F and Gallinger S. Defective mismatch repair as a predictive marker for lack of efficacy of fluorouracil-based adjuvant therapy in colon cancer. J Clin Oncol 2010; 28: 3219-3226.
[17] Boland CR, Thibodeau SN, Hamilton SR, Sidransky D, Eshleman JR, Burt RW, Meltzer SJ, Rodriguez-Bigas MA, Fodde R, Ranzani GN and Srivastava S. A National Cancer Institute Workshop on Microsatellite Instability for cancer detection and familial predisposition: development of international criteria for the determination of microsatellite instability in colorectal cancer. Cancer Res 1998; 58: 5248-5257.
[18] Amin MB, Greene FL, Edge SB, Compton CC, Gershenwald JE, Brookland RK, Meyer L, Gress DM, Byrd DR and Winchester DP. The Eighth Edition AJCC Cancer Staging Manual: Continuing to build a bridge from a population-based to a more "personalized" approach to cancer staging. CA Cancer J Clin 2017; 67: 93-99.
[19] Murphy CC and Zaki TA. Changing epidemiology of colorectal cancer - birth cohort effects and emerging risk factors. Nat Rev Gastroenterol Hepatol 2024; 21: 25-34.
[20] Wang C, Zhang H, Liu Y, Wang Y, Hu H and Wang G. Molecular subtyping in colorectal cancer: a bridge to personalized therapy (Review). Oncol Lett 2023; 25: 230.
[21] Ho V, Chung L, Wilkinson K, Ma Y, Rutland T, Lea V, Lim SH, Abubakar A, Ng W, Lee M, Roberts TL, Becker TM, Mackenzie S, Chua W and Lee CS. Microsatellite instability testing and prognostic implications in colorectal cancer. Cancers (Basel) 2024; 16: 2005.
[22] Nan B, Pan Y, Ge Y, Sun M, Cai J and Kan X. Preliminary study on the evaluation value of extracellular volume fraction in the pathological grading of lung invasive adenocarcinoma. Curr Med Imaging 2025; 21: e15734056392707.

[23] Nishimuta Y, Tsurumaru D, Kai S, Maehara J, Asayama Y, Oki E and Ishigami K. Extracellular volume fraction determined by equilibrium contrast-enhanced computed tomography: correlation with histopathological findings in gastric cancer. Jpn J Radiol 2023; 41: 752-759.
[24] Wang Q, Yu M and Zhang S. The characteristics of the tumor immune microenvironment in colorectal cancer with different MSI status and current therapeutic strategies. Front Immunol 2025; 15: 1440830.
[25] Ros J, Baraibar I, Saoudi N, Rodriguez M, Salvà F, Tabernero J and Élez E. Immunotherapy for colorectal cancer with high microsatellite instability: the ongoing search for biomarkers. Cancers (Basel) 2023; 15: 4245.
[26] Evrard C, Messina S, Sefrioui D, Frouin É, Auriault ML, Chautard R, Zaanan A, Jaffrelot M, De La Fouchardière C, Aparicio T, Coriat R, Godet J, Silvain C, Randrian V, Sabourin JC, Guimbaud R, Miquelestorena-Standley E, Lecomte T, Moulin V, Karayan-Tapon L, Tachon G and Tougeron D. Heterogeneity of mismatch repair status and microsatellite instability between primary tumour and metastasis and its implications for immunotherapy in colorectal cancers. Int J Mol Sci 2022; 23: 4427.
[27] Küçükköse E, Baars MJD, Amini M, Schraa SJ, Floor E, Bol GM, Borel Rinkes IHM, Roodhart JML, Koopman M, Laoukili J, Kranenburg O and Vercoulen Y. Stromal localization of inactive CD8+ T cells in metastatic mismatch repair deficient colorectal cancer. Br J Cancer 2024; 130: 213-223.
[28] Gerber BL. Assessment of the extracellular matrix by CT extracellular volume fraction. JACC Cardiovasc Imaging 2024; 17: 529-532.
[29] Fujiyoshi K, Yamaguchi T, Kakuta M, Takahashi A, Arai Y, Yamada M, Yamamoto G, Ohde S, Takao M, Horiguchi SI, Natsume S, Kazama S, Nishizawa Y, Nishimura Y, Akagi Y, Sakamoto H and Akagi K. Predictive model for high-frequency microsatellite instability in colorectal cancer patients over 50 years of age. Cancer Med 2017; 6: 1255-1263.
[30] Cesmecioglu Karavin E, Sağnak Yılmaz Z, Yazici H, Ersoz S and Mungan S. Comparison of microsatellite instability with clinicopathologic data in patients with colon adenocarcinoma. Cureus 2024; 16: e57814.
[31] Lu J, Tan H, Guo T, Chen X and Tong Z. Association between microsatellite instability status, clinicopathological features and mitochondrial DNA amplification in patients with colorectal cancer. Oncol Lett 2024; 28: 564.
[32] Hakki L, Khan A, Gonen M, Stadler Z, Segal NH, Shia J, Widmar M, Wei IH, Smith JJ, Pappou EP, Nash GM, Paty PB, Garcia-Aguilar J and Weiser MR. Lymph node metastases and associated recurrence-free survival in microsatellite stable and unstable colon cancer. Ann Surg Oncol 2023; 30: 8487-8494.
[33] Wang K, Zhou S, Wang H, Zhang X, Cheng W, Sun Y, Ding C and Guan W. The influence of microsatellite status on tertiary lymphoid structures and lymph node metastasis in colorectal cancer. Clin Transl Oncol 2025; 27: 4214-4220.